Front. Optoelectron. 2016, 9(2): 225–237
DOI 10.1007/s12200-016-0624-1

REVIEW ARTICLE

Novel types of photonic band crystal high power and high brightness semiconductor lasers

Md. Jarez MIAH (✉)[1], Vladimir P. KALOSHA[1], Ricardo ROSALES[1], Dieter BIMBERG[1,2]

1 Institute of Solid State Physics, Technical University of Berlin, Hardenbergstrasse 36, 10623 Berlin, Germany
2 King Abdulaziz University, Jeddah, Kingdom of Saudi Arabia (KSA)

Abstract A novel type of high power edge-emitting semiconductor laser (SL) with extended vertical photonic band crystal (PBC) waveguide was reviewed. Simulations predict narrow beam divergence, resulting from the thick PBC waveguide, to be independent of realistic variations of the growth parameters. Narrow ridge lasers fabricated along the simulations indeed demonstrate superior output power, narrow beam divergence, circular beam profile, excellent beam quality and very low astigmatism. Efficient fiber coupling decisive for most applications was thus eased. Stability of the laser under a wide range of operating temperature was demonstrated. Ultrashort pulses with few ps of duration at GHz repetition rates were generated by passively mode locking the lasers.

Keywords semiconductor laser (SL), edge-emitting laser, high brightness laser, narrow beam divergence, high peak power pulses

1 Introduction

The demand for high brightness semiconductor lasers (SLs) for a rapidly increasing number of applications as pump sources for solid state and fiber lasers, spectroscopy, medicine, material processing, has recently stimulated much research into novel designs and better exploitation of traditional ones. Such lasers, single ones or coupled bars, offer compactness, large energy efficiency and low cost of chip fabrication [1–4]. Narrow optical pulses from such lasers with repetition frequency in the gigahertz (GHz) range are additionally attractive for different applications like frequency conversion for display applications, or time-resolved spectroscopy.

High output power combined with fundamental mode emission in both transverse directions parallel (lateral) and vertical to the growth direction are prerequisite for high-brightness and thus decisive for material processing, like cutting and welding (Fig. 1) [5]. Conventional edge-emitting SLs have a simple vertical waveguide, which consists of a thin active region of several tens of nanometer thickness, and two surrounding cladding layers (Fig. 2). Maximum output power from these lasers is limited by their small emitting area due to their tightly confined optical fields in the thin active region. Resulting high optical power density at the facets causes catastrophic optical mirror damage (COMD) [6] if the power density exceeds 10–20 MW/cm^2. An increase of the emission area by expanding the optical fields in both lateral and vertical directions can reduce the power density at the facets and, consequently, increase the output power. Typical high-power SLs extend their ridges in lateral direction up to several hundreds of micrometers. However, such widening of ridges leads to the emission of a multitude of higher order modes, deteriorating the lateral beam quality and hindering high brightness. Moreover, as illustrated in Fig. 2, due to the asymmetric lasing area in conventional lasers, the emitted beam suffers from a high elipticity with large vertical beam divergence, typically 30°–60° full width at half maximum (FWHM). Such asymmetric and large beam divergence require complex and costly optics with large numerical aperture for focusing or efficient fiber coupling. Therefore, development of SLs combining all demanded features, e.g., high output power, good beam quality and narrow beam divergence in both lateral and vertical directions, still presents a challenge for present research.

2 High power laser concepts

So far, a series of approaches have been presented to achieve high output power by avoiding COMD. All the approaches aim to reduce the power density at the facets by

Received February 9, 2016; accepted February 25, 2016

E-mail: jarez.miah@tu-berlin.de

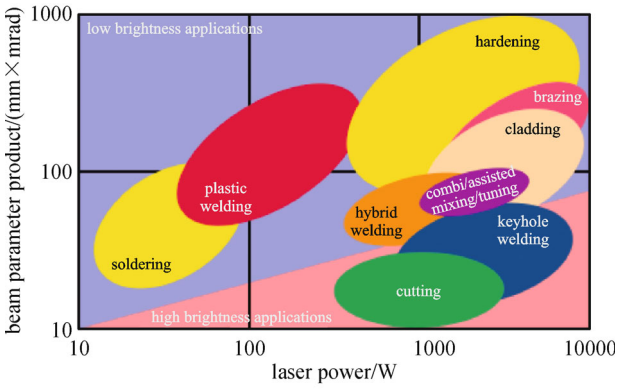

Fig. 1 Beam parameter product and laser power requirement for different material processing applications [5]

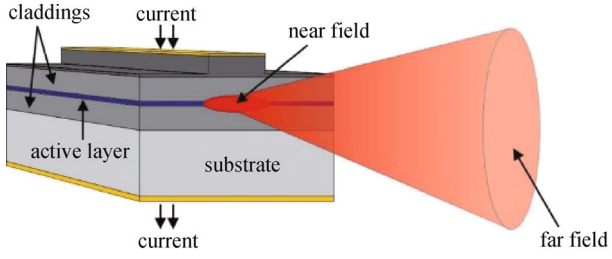

Fig. 2 Schematic drawing of a conventional edge-emitting laser with broad vertical beam divergence

expanding the optical field by broad vertical and/or lateral emitting areas [7–20]. A so-called T^3 (thin tapered-thickness) laser uses thinner active layer near both mirrors than in the inner region [7]. This allows the optical fields to penetrate more into the surrounding cladding layers and reduces both vertical beam divergence and power density at the facets. As narrow as 10° FWHM vertical beam divergence and 120 mW continuous-wave (CW) output power in fundamental transverse mode are reported at 780 nm [7].

A pair of specially designed low-index [8–10] or high-index [11] mode expansion layers on both sides of the active region can broaden the optical fields in the epitaxial layer stack. The thicknesses and the refractive indices of the expansion layers are carefully chosen to be similar to the effective refractive index of the lasing mode. FWHM vertical beam divergence of 13° and 24° are reported at 980 nm [9] and 650 nm [11] using low-index and high index mode expansion layers, respectively. A very thick mode expansion layer incorporated only on one side of the active region also provides a FWHM vertical beam divergence of only 11–12° and 500 mW CW output power in single transverse mode at 980 nm [12].

Vertical mode expansion using a large optical cavity along with low refractive index contrast between active layers and surrounding waveguide layers is reported in Refs. [13–15]. 12 W CW output power with vertical beam divergence of 15° (95% power content) in the vertical fundamental mode is delivered at 1060 nm for broad area lasers [15].

Less than 1° FWHM vertical beam divergence and 3.3 W CW output power are achieved at fundamental vertical mode emission at 1060 nm from tilted waveguide lasers [16]. In this approach, the optical mode from the narrow waveguide containing active layers is allowed to leak into the thick transparent substrate via a thin cladding layer. The opposite side of the substrate is polished and provides mirror-like reflection to the leaky mode. The commonly unused thick substrate is used as a broad waveguide for the guided leaky mode.

Lateral waveguiding approaches combine a tapered structure with a ridge waveguide along the longitudinal direction [17–20]. Tightly guided optical fields in the ridge waveguide region are expanded in the tapered section, reducing the optical load at the output facets and enabling larger output power. The narrow ridges define a very good beam quality which consequently results in very high brightness. A CW output power of 3.5 W and a brightness as high as 255 MW/cm^2/sr are achieved at 1040 nm [17].

3 Photonic band crystal (PBC) concept and layer structure design

A different approach for vertical mode expansion utilizing a highly asymmetric vertical waveguide, called a PBC waveguide, has been proposed [21–23]. A schematic drawing of a PBC edge-emitting lasers is shown in Fig. 3. Instead of a simple lower cladding layer like in conventional lasers (cf. Fig. 2), PBC lasers consist of a sequence of quasi-periodic epitaxial layers followed by a defect layer, which terminates the periodicity of the layer stack. Quantum wells (QWs) are placed within the defect layer. The thicknesses and the contents of the PBC layers are chosen to localize only the fundamental mode in the active region and delocalize all the higher order modes. Broad extension of the fundamental mode gives rise to narrow vertical beam and the typical elliptic beam profile of conventional lasers also turns into a nearly circular one. The reduced facet load allows larger output power before reaching the threshold power density for COMD. Fundamental mode emission in vertical direction necessary for high brightness applications is assured by following improved mode selection criteria. The fundamental mode is localized in the active region and shows a better confinement factor than the delocalized higher order modes. A spatially modulated doping profile is employed with higher doping concentration near the substrate where the maxima of the higher order modes are located. Thus the higher order modes suffer larger free carrier absorption losses than the fundamental one. The loss discrimination is

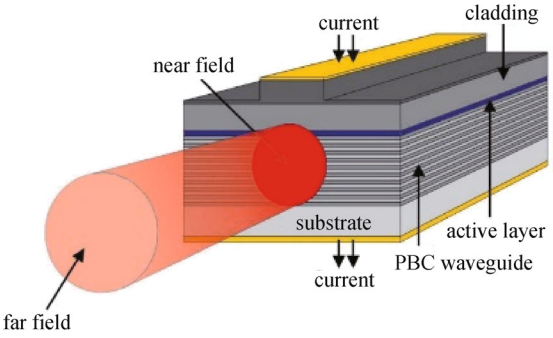

Fig. 3 Schematic drawing of a PBC laser with narrow vertical beam divergence [34]

further enhanced by introducing higher leakages of the higher order modes into the substrate by controlling thickness and composition of the layer closest to the substrate. The combination of higher confinement factor, lower free carrier absorption and leakage losses of the fundamental mode highly favors its emission over the higher order counterparts.

The concept of PBC lasers has been successfully realized for a wide range of emission wavelengths [22–34] and recently transformed to the concept of high-brightness broad-area edge-emitting (HIBBEE) lasers, where the waveguide shows no regularity of repeating layers any more [35].

In this paper, several generations of 1060 nm PBC lasers with varying total vertical thickness and different number of interfaces in the PBC waveguide are reviewed and compared to each other in detail. Divergence of each structure estimated from simulation is compared to experimental results. Record single transverse mode output power of 1.9 W for 1060 nm ridge waveguide (RW) lasers with beam quality factor M^2 below 2 and a very low astigmatism of 5 – 14 μm are obtained from RW lasers. More than 9 W output power from broad area (BA) lasers under CW operation is reported. FWHM vertical beam divergence as narrow as 7° is obtained from the BA laser. Ultra-short pulses providing peak power of 3 W and highest to date peak brightness of 180 MW/cm^2/sr for 1060 nm lasers by passive mode-locking are presented. An approach to reduce series resistivity and thus to improve power conversion efficiency (PCE) of thick PBC lasers is simulated and proved by experiments. RW lasers having this optimized PBC waveguide provide a perfectly circular beam emission for 1.3 W CW output power with 16° FWHM beam divergence in both transverse directions.

4 Results

Three generations of 1060 nm PBC lasers having 15, 9 and 6 pairs of quasi-periodic layers in the PBC waveguide having a total vertical thickness of 15, 12 and 10 μm are investigated. Structures are named A, B and C below, respectively. In all cases, the epitaxial layers are grown on n-doped (001) oriented GaAs substrates using metal-organic vapor phase epitaxy. Four InGaAs/GaAsP QWs are tuned for an emission wavelength of 1060 nm. The structures are cleaved into both BA and RW lasers with different cavity lengths. BA lasers have 100 μm wide ridge and unpassivated/uncoated facets. While the RW lasers have varying ridge widths from 5 to 9 μm. Ridges in RW lasers are surrounded by two deep-etched trenches where all the epitaxial layers are etched away leaving only 100 nm of the p-doped side above active region. Both BA and RW lasers are characterized in pulsed and CW mode. 800 ns pulses at a repetition rate of 1 kHz are used for pulsed operation. For CW characterizations, the lasers are mounted down on CuW heat spreader and Cu mounts. In some cases, facets of the RW lasers are also passivated and coated with high reflection (HR) and antireflection (AR) coatings of 95% and 5% reflectivities, respectively.

4.1 PBC waveguide with 15 pairs of PBC layers (structure A)

Figure 4(a) shows a schematic of a 1060 nm PBC laser. In the n-doped side, the laser structure has 15 pairs of AlGaAs layers with alternating Al contents and a total vertical thickness of approximately 15 μm. The refractive index profile along the vertical direction is presented in Fig. 4(b). The selected Al contents and thicknesses of the AlGaAs layers give rise to spreading tail of the fundamental mode towards the substrate while localizing its maximum at active region. The broad fundamental near-field results in a narrow far-field distribution with only 7.5° FWHM vertical beam divergence (Fig. 4(c)). The calculated combined leakage and free carrier absorption losses and optical confinement factor of first 20 modes are depicted in Fig. 4(d). The emitted laser beam is estimated to contain a dominating fundamental mode with at least five times larger confinement factor and an order of magnitude less loss. The robustness of similar type of a thick PBC laser structure against the unintentional deviations of the refractive indices of QWs, thicknesses and alloy compositions of the PBC layers are discussed in Ref. [30]. Although, the lasers presented there are designed for emission wavelength of 980 nm, the current structures for 1060 nm emission wavelength are also expected to behave in a similar fashion.

Internal parameters of the structure are determined from pulsed measurements of BA lasers with different cavity lengths L at $T = 20$°C (see Fig. 5). A high internal quantum efficiency $\eta_{\text{int}} = 93\%$, low internal loss $\alpha_{\text{int}} = 1.3$ cm^{-1}, threshold modal gain $\Gamma g_0 = 24$ cm^{-1} and low threshold current density (at $L = \infty$) $J_\infty = 243$ A/cm^2 are obtained.

The sensitivity of the lasers on temperature is evaluated by determining characteristic temperature T_0 of a 1.5 mm

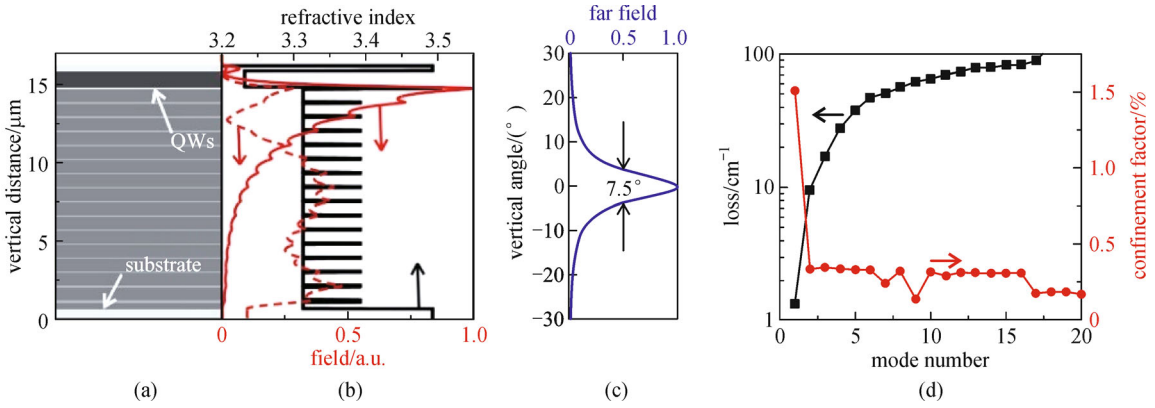

Fig. 4 (a) Schematic drawing of layer structure of a 1060 nm PBC laser with 15 pairs PBC layers; (b) refractive index (solid line, top axis) and calculated near-field distributions of the fundamental (solid line, bottom axis) and first higher order (dashed line, bottom axis) mode along vertical distance; (c) calculated far-field distribution of the fundamental mode; (d) calculated optical loss (square) and confinement factors (circle) of the first 20 modes [32]

long BA laser as illustrated in Fig. 6. Output power-current (*L-I*) characteristics of the laser is measured at *T* from 0°C to 80°C. With increasing *T*, threshold current density J_{thr} continuously increases and slope efficiency of the laser decreases due to increased carrier leakage, non-radiative Auger combination and reduced material gain [36,37]. T_0 is calculated from logarithmic dependence of J_{thr} on *T* (Fig. 6 (inset)). A high $T_0 = 200$ K conforming a stable threshold behavior of the laser is obtained within 0 – 25°C temperature range. T_0 decreases to 93 K above 25°C.

Vertical far-field distribution of a 3.0 mm long BA laser with unpassivated and uncoated facets is shown in Fig. 7 in CW mode at $I = 5.0$ A and $T = 20$°C. FWHM beam divergence angle of 7.3° perfectly agree with the estimated value from simulation (cf. Fig. 4). The laser provide a thermally limited 9.5 W maximum output power and 40% maximum PCE in CW mode and emits in the range of 1060 nm wavelength as depicted in the insets. The thermal roll-over in the *L-I* curve occurs due to the increased heating of the laser at higher currents. With increasing operating current, power dissipation in the laser increases which rises its internal temperature and decreases current injection efficiency due to increased carrier leakage. Thus a strong reduction in output power at higher currents and, subsequently, a roll-over is appeared.

Light-current-voltage (*L-I-V*) and corresponding PCE of a 5 μm and a 9 μm wide RW laser both having 2.64 mm long cavity are shown in Fig. 8(a). Laser facets are passivated and coated with HR/AR coatings. Maximum output powers of 1.6 and 2.4 W, and a maximum PCE of 37% and 38% are obtained with 5 and 9 μm wide lasers, respectively. 5 μm wide RW lasers provide single transverse mode emission with bell-shaped and single lobed far-field distributions across the whole operating range. Lateral and vertical far-field distributions along with their Gaussian fits at $I = 2.0$ A are presented in Fig. 8(b). FWHM beam divergence of as narrow as 9° in lateral and 13° in vertical direction are observed. 9 μm wide RW laser

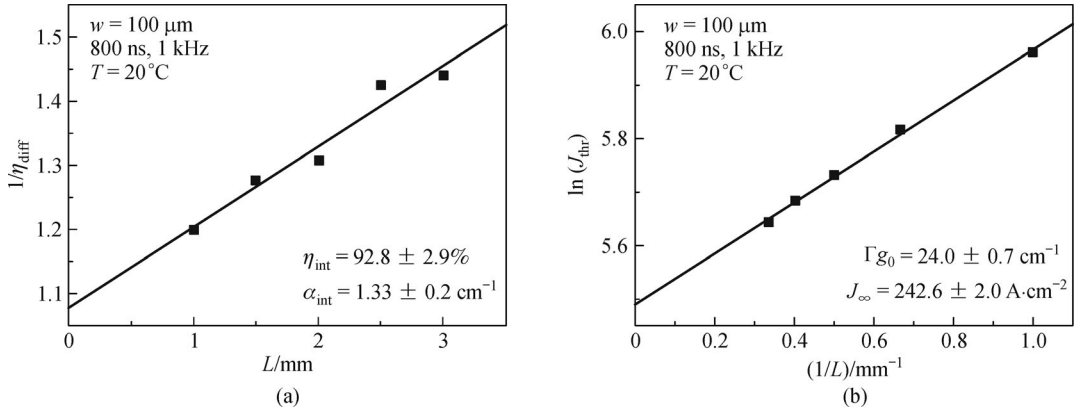

Fig. 5 Cavity length dependence of reciprocal differential quantum efficiency (a) and threshold current density (b) of BA lasers at $T =$ 20°C in pulsed mode [32]

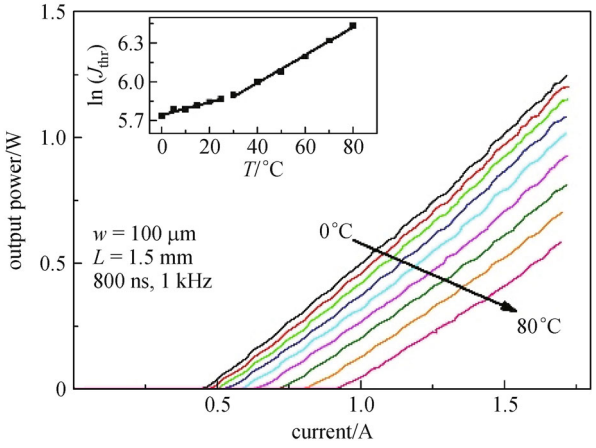

Fig. 6 *L-I* characteristics of a 1.5 mm long BA laser at T = 0°C to 80°C in steps of 10°C in pulsed mode. Inset shows the corresponding threshold current density of the laser as a function of T

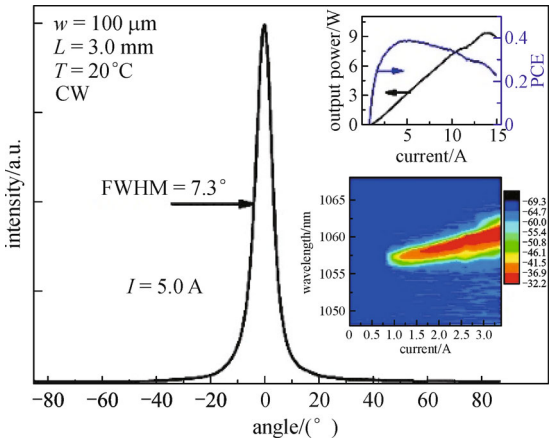

Fig. 7 Vertical far-field distribution of a 3.0 mm long BA laser at T = 20°C in CW mode at I = 5.0 A. Inset shows the output power and corresponding PCE (upper) and emission spectrum (lower) of the laser as a function of drive current

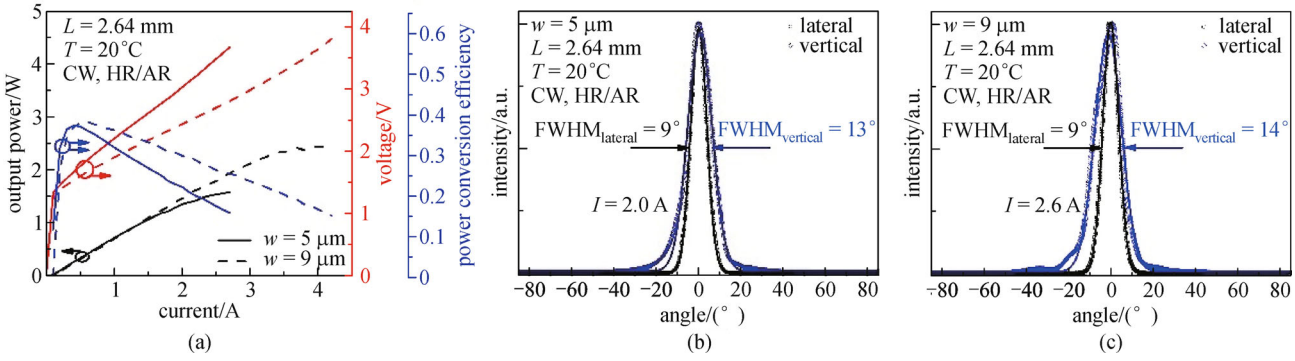

Fig. 8 (a) *L-I-V* characteristics and corresponding PCEs of a 5 μm and a 9 μm wide and 2.64 mm long RW lasers in CW mode at T = 20°C. Far-field distributions along with their Gaussian fits of the 5 μm (b) and 9 μm (c) wide RW laser in lateral and vertical directions at I = 2.0 and 2.6 A, respectively. FWHM beam divergence angles are indicated. The lasers are HR/AR coated

yields single transverse mode emission with 9° and 14° FWHM beam divergences in lateral and vertical directions, respectively, with corresponding output power of 1.9 W (Fig. 8(c)). The power represents highest ever reported single transverse mode output power for 1060 nm RW lasers [32,38].

Beam quality of the lasers is evaluated by measuring beam quality parameter M^2 according to the 4-σ (standard deviation) method. In the beam profiling system, the laser beam is directed through a lens to focus to an artificial beam waist. M^2 is then calculated from measured beam width versus distance plot. Astigmatism is calculated from the distance of the beam waist locations along the vertical and lateral directions. Figure 9(a) shows the measured lateral and vertical M^2 of the 5 μm wide RW laser at T = 20°C in CW mode. Over entire operating current range, M^2 remains well below 1.8 in both transverse directions. A slight increase in lateral M^2 at higher currents implies larger deviations of the laser beams from Gaussian shape and occurs due to increased contribution from higher order modes in laser emission. A maximum brightness B of 60 MW/cm^2/sr is obtained at I = 1.6 A. Maximum brightness increases to 72 MW/cm^2/sr in case of 9 μm wide RW laser as illustrated in Fig. 9(b). Measured astigmatism stays within 5 to 14 μm over the whole operating current range.

The thermal stability of the laser performances are investigated by measuring *L-I-V*, M^2 and astigmatism of a 6 μm wide RW laser at different T from 20°C to 80°C. Figure 10(a) presents *L-I-V* curves of the laser. With increasing T, maximum output power decreases from 1.8 W at 20°C to still more than 1.3 W output power at 80°C and maximum PCE declines from 34% to 30%. The decrease of output power and PCE is the consequence of continuous increase of J_{thr} and decrease of η_{diff} with T. Figure 10(b) shows measured M^2 in both lateral and vertical directions and astigmatism at different drive

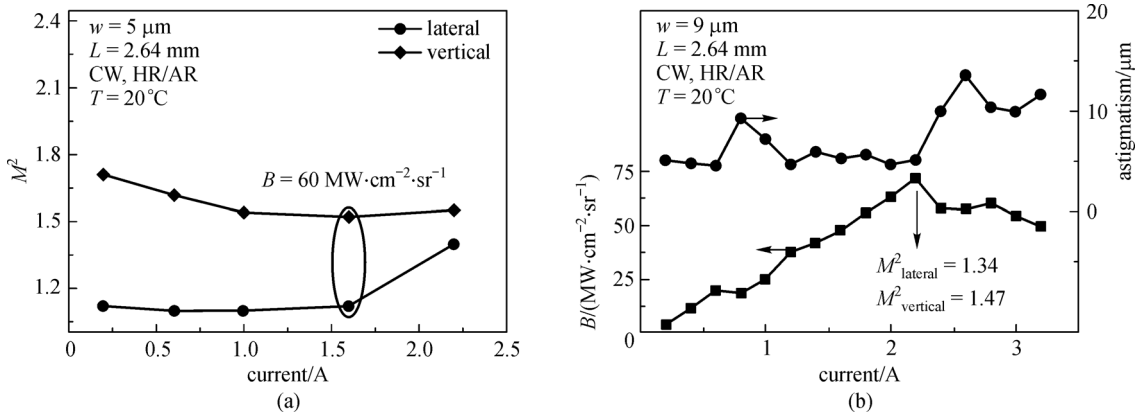

Fig. 9 (a) Lateral and vertical M^2 of the 5 μm wide RW laser from Fig. 8 as a function of drive current in CW mode. Maximum brightness B is indicated; (b) brightness and astigmatism of the 9 μm wide RW laser versus drive current in CW mode at $T = 20$°C. M^2_{lateral} and M^2_{vertical} at maximum brightness are indicated

currents. Vertical M^2 remains within 1.5–1.9 at all investigated temperature over entire operating current range. While an increasing lateral M^2 with increasing temperature is observed, almost constant M^2 is maintained for each temperature up to I = 2.2 A. Thereafter, an increase in M^2 is observed at all different temperature which is the evidence of increased contribution of higher order modes. However, still a very good beam quality with $M^2 < 2$ is achieved up to the highest operating current. A stable anastigmatic behavior, with astigmatism varying only from 0.5 to 2 μm, is also observed at all different temperatures (Fig. 10(c)).

4.2 PBC waveguide with 9 pairs of PBC layers (structure B)

A different PBC structure consisting of 9 pairs of alternating PBC layers and a total thickness of 12 μm is investigated in the passive mode locking regime. Figure 11 shows the refractive index profile, calculated near field distributions of the fundamental and first higher order modes, calculated far-field distribution of the fundamental mode, calculated total optical loss and confinement factor of the first 20 modes. Similar to the structure A, thicknesses and contents of the PBC layers are chosen to ensure an order of magnitude less optical loss and five times better confinement factor of the fundamental mode as compared to that of the higher order modes. Simulated FWHM vertical far-field divergence is 7.3°.

Basic pulsed mode characterization of the structure is shown in Fig. 12. Extracted parameters from cavity length dependence of differential quantum efficiency and threshold current are: $\eta_{\text{int}} = 94\%$, $\alpha_{\text{int}} = 1.4$ cm^{-1}, $\Gamma g_0 = 32$ cm^{-1} and $J_\infty = 230$ A/cm^2.

For passively mode locked operation of the PBC lasers, RW lasers with two isolated sections, i.e., gain and saturable absorber sections, are processed. Different ratio of lengths of gain to absorber sections are studied. The lasers are as-cleaved and mounted p-side up on Cu-mounts. Mode locking in the devices are investigated using two different measurement techniques: second-harmonic generation (SHG) based autocorrelation technique, and recording laser radio frequency (RF) spectra.

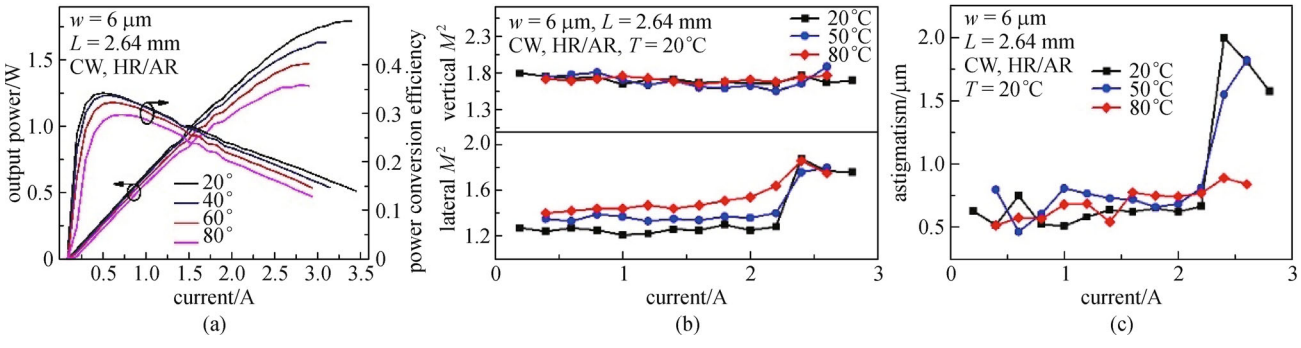

Fig. 10 (a) *L-I* curves and corresponding PCEs of a 6 μm wide and 2.64 mm long RW laser at $T = 20$°C to 80°C in 20°C steps; (b) lateral (bottom) and vertical (top) M^2 of the laser as a function of drive current at different T; (c) measured astigmatism of the laser at different T versus drive current. The laser is HR/AR coated. All the measurements are performed in CW mode [34]

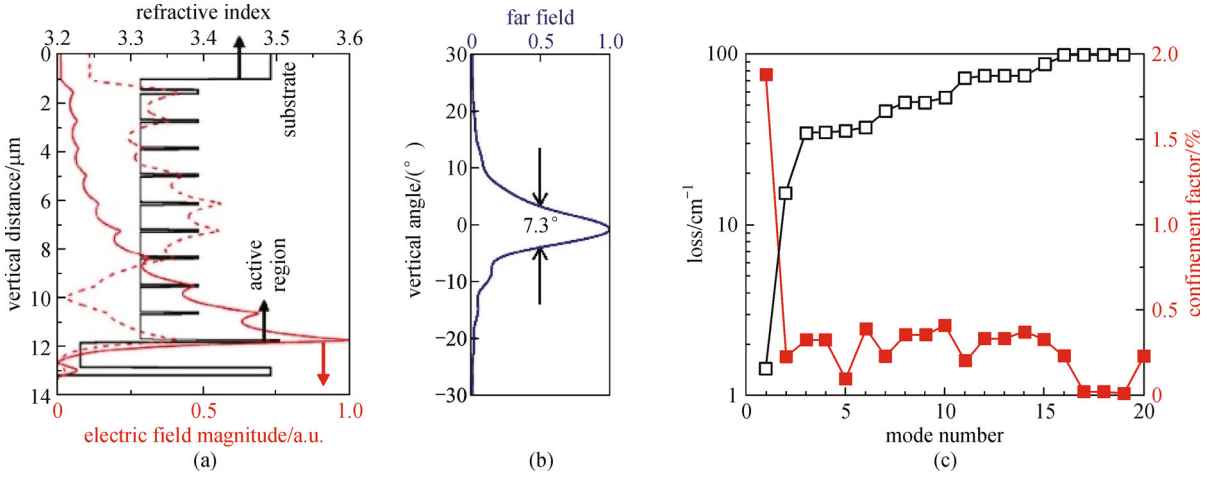

Fig. 11 (a) Refractive index (solid line, top axis) and calculated near-field distributions of the fundamental (solid line, bottom axis) and first higher order (dashed line, bottom axis) mode along vertical distance; (b) calculated far-field distribution of the fundamental mode; (c) calculated optical loss (empty square) and confinement factors (filled square) of the first 20 modes [33]

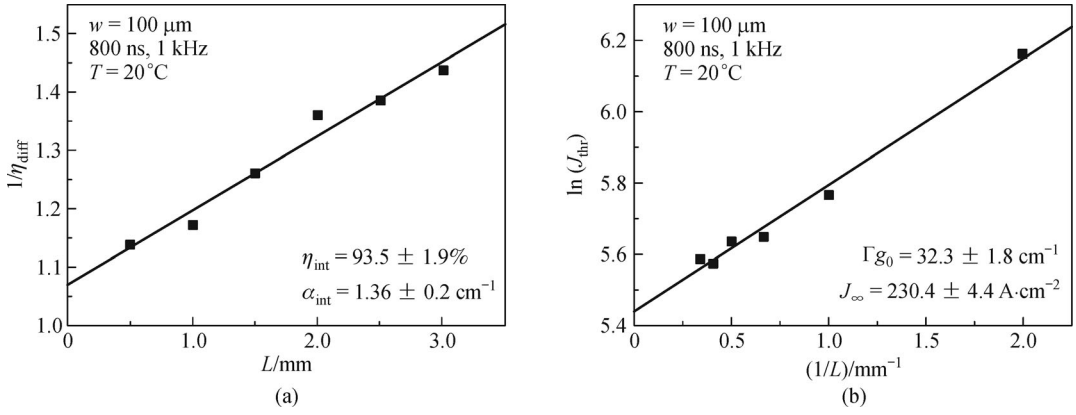

Fig. 12 Reciprocal differential quantum efficiency as a function of cavity length (a) and dependence of threshold current density on inverse cavity length (b) [33]

Figure 13 illustrates the far-field distribution of a 5 μm wide and 1.0 mm long single-section (only gain section) RW laser in CW mode at I = 0.5 A. The laser provides single-lobed bell-shaped far-field distributions with FWHM beam divergence of 6° in lateral and 9° in vertical direction.

Figure 14 shows the intensity distributions of second harmonics of two section RW lasers for three different total cavity lengths with a fixed gain to absorber length ratio of 12:1. FWHM pulse durations are determined after deconvolution assuming Gaussian pulse shape. Minimum pulse durations of 6, 11 and 15 ps are obtained at fundamental repetition frequency of 24, 15 and 5 GHz with 1.8, 2.8 and 8.5 mm long cavity lasers, respectively. The broadening of the pulses with increasing cavity length is attributed to the increased (1) intracavity dispersion in longer devices and (2) pulse instability due to increased number of round trips necessary for mode locking.

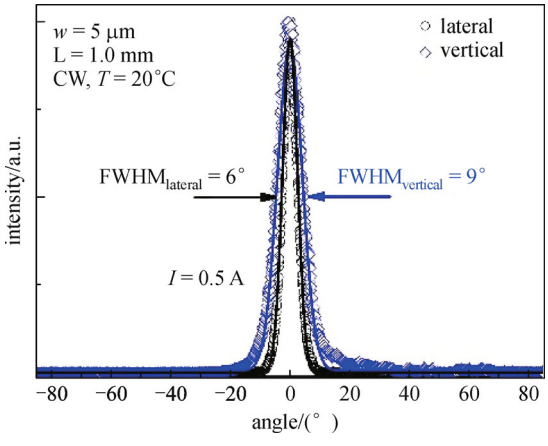

Fig. 13 Far-field distributions of a 5 μm wide and 1.0 mm long single-section RW laser at I = 0.5 A [33]

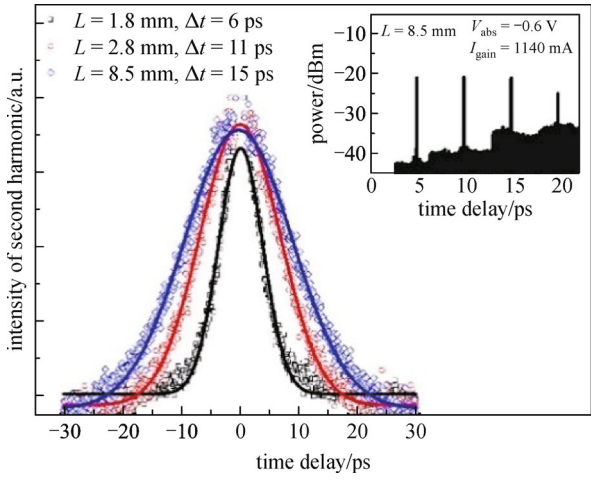

Fig. 14 Intensity distributions of second harmonics and their Gaussian fits for two section RW lasers with total cavity lengths of 1.8, 2.8 and 8.5 mm. FWHM pulse durations Δt are indicated. Inset shows RF spectrum of the 8.5 mm long laser at V_{abs} = –0.6 V and I_{gain} = 1140 mA [33]

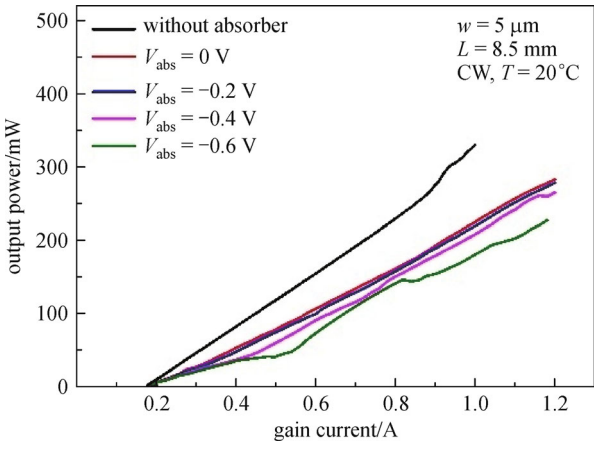

Fig. 15 Output power of a 5 μm wide and 8.5 mm long two-section RW laser at different absorption voltages as a function of gain current

Measured RF spectrum of 8.5 mm long mode-locked laser at forward current I_{gain} = 1140 mA in gain section and reverse bias voltage V_{abs} = –0.6 V in absorber section is illustrated in Fig. 14 (inset). Sharp peaks at the fundamental mode-locking frequency of 5 GHz and at its harmonics are clear indication of mode-locking operation.

Figure 15 presents the output power as function of gain current I_{gain} of the 8.5 mm long RW laser at different bias voltages for absorption section. At I_{gain} = 1140 mA and V_{abs} = –0.6 V, the laser provides a maximum average power of 215 mW and correspondingly a peak power of as high as 3 W. Beam quality parameter M^2 varies within 1.15–1.20 in lateral and 1.2–1.25 in vertical directions up to maximum investigated current. These result in a highest to date pulse brightness of 180 MW/cm^2/sr for electrically pumped and passively mode-locked lasers at 1060 nm wavelength range.

4.3 PBC waveguide with 6 pairs of PBC layers (structure C)

The structures A and B presented above suffer from high electrical series resistance which limits their maximum PCE to 40%. The resistivity of such PBC structure with thick waveguide with alternative layer compositions is controlled by the doping profile as well as the number of interfaces between the epitaxial layers. Barriers at the hetero interfaces hamper vertical transport, an effect which is especially severe for distributed Bragg reflector (DBR) mirrors in VCSELs with a large band offset [39]. That is why, a new PBC structure with relatively thinner vertical waveguide of 10 μm and reduced number of only 6 pairs of PBC layers is studied. The lasers still provide narrow vertical beam divergence but considerably reduced series resistance.

Figures 16 (a)–16(c) show the Al composition of the epitaxial layers along vertical distance, calculated near field distributions of the fundamental and first higher order modes and doping profile of donors and acceptors. Calculated far-field distributions shows a slight increase in FWHM vertical beam divergence than structures A and B, which is attributed to the reduced total thickness of structure C (Fig. 16 (d)). A comparative calculations of the current versus applied voltage through both the present structure C and structure A were performed and the series resistivities ρ_s were extracted by linear fitting of current-voltage curves in the high current regime (Fig. 17). Figure 17(a) shows the effect of doping level in the interface layers on the carrier transport. Higher doping level of 2×10^{18} cm^{-3} in the interface layers substantially decreases the series resistance for both structures as compared to the case when doping is the same as in adjacent layers above and below the interfaces. The optimum thickness of the interface layer is revealed by simulating the series resistance for different thicknesses with a doping level of 2×10^{18} cm^{-3} (Fig. 17 (b)). Linearly graded interface layers of thickness 20 nm with high doping minimize the negative influence of varying Al content in the layers on current transport through the multi-layer structures. For 20-nm thick interface layers, the fundamental mode remains extended over the whole vertical structure to provide narrow far field beam profile. We note also that high doping of thin interface layers causes insignificant increase of free carrier absorption losses and does not affect the lasing efficiency.

Figure 18 illustrates the extracted internal parameters of the structure to be η_{int} = 83%, α_{int} = 1.7 cm^{-1}, Γg_0 = 34 cm^{-1} and J_∞ = 208 A/cm^2. The relatively low internal efficiency is caused by non-radiative recombination processes due to a non-optimum ramping from the low growth temperature used for the active region to the higher

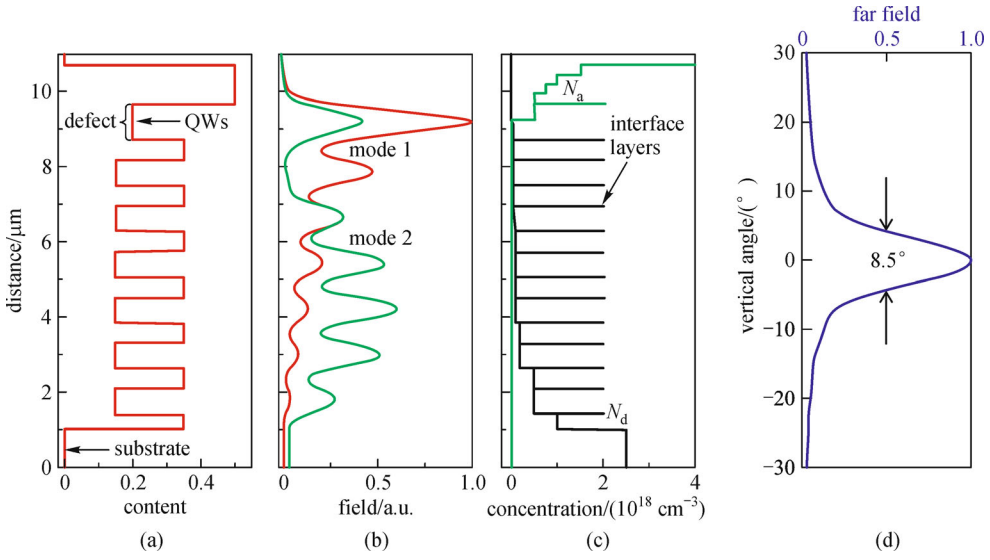

Fig. 16 (a) Al content versus vertical distance of the laser structure containing 6 pairs of alternating epitaxial layers and a defect layer with four QWs; (b) simulated near-field amplitude of the fundamental mode 1 (red curve) and the first higher order mode 2 (green); (c) doping concentrations N_d and N_a of the Si donors (black) and C acceptors (green), respectively, with high doping of the graded interface layers; (d) calculated far-field distribution of the fundamental mode

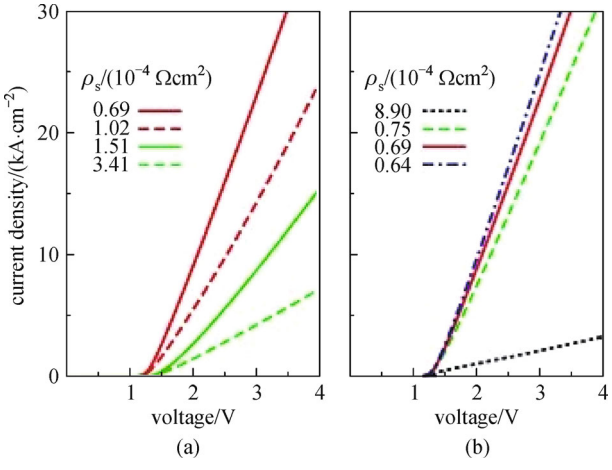

Fig. 17 Comparison of the calculated current density versus drive voltage (a) for the structure C with 6 pairs (red curves) and structure A with 15 pairs (green) of alternating layers, 20 nm thick interface layers with the same doping level as in the adjacent layers (dashed) and a doping level of 2×10^{18} cm^{-3} (solid); (b) for the structure with 6 pairs of alternating layers and interface layers with a doping level 2×10^{18} cm^{-3} for thickness 0 nm (abrupt) (black dotted curve), 10 nm (green dashed), 20 nm (red solid), 50 nm (blue dotted-dashed)

growth temperature of the p-waveguide. Similar to structures A and B, further optimization of the growth temperature is expected to improve the internal efficiency of structure C to close to 100%.

Figure 19(a) shows *L-I-V* characteristics and the corresponding PCEs of 5 and 9 μm wide RW lasers both with a cavity length of 2.64 mm in CW mode at $T = 20$°C. The laser facets are passivated and coated with HR and AR coatings. A thermally limited maximum output power of 1.3 and 2.1 W and maximum PCE of 34% and 36% are achieved from 5 and 9 μm wide lasers, respectively. The 9 μm wide laser has a series resistivity of $\rho_s = 0.45\ (\pm0.01) \times 10^{-4}\ \Omega\cdot\text{cm}^2$. Previously reported 9 μm wide RW lasers from structure A show a more than 3 times higher series resistivity of $\rho_s = 1.36\ (\pm0.02) \times 10^{-4}\ \Omega\cdot\text{cm}^2$ (cf. Fig. 8). The measured resistivity values agree well with the theoretical results. Despite the relatively low internal efficiency $\eta_{int} = 83\%$, the maximum PCE is similar to that of the structure A entirely because of lower ρ_s. The lower total thickness and the lower number of layers in structure C also make the growth process less demanding and reduce wafer bow. Similar to the structure A, the present 9 μm wide lasers provide a slightly elliptic beam with single-lobed far-field in both lateral ($\theta_{FWHM} = 16°$) and vertical ($\theta_{FWHM} = 19°$) directions up to 1.9 W output power (Fig. 19(b)). The lateral far-field patterns contain some additional local peaks. Due to the finite width of the trenches surrounding the ridge, radiation leaks into the outer high-index regions [40]. The propagation of the leaked radiation inside the cavity gives rise to those peaks in the far-fields.

A perfectly circular beam profile is obtained with 5 μm wide RW lasers still at highest output power. Far-field distributions at different operating currents in CW mode at $T = 20$°C for the 5 μm wide RW laser are shown in Figs. 20 (a)–20(d). FWHM beam divergence angles in both lateral and vertical directions are plotted in Fig. 20(e). A bell-shaped single-lobed far-field distribution is obtained in both lateral and vertical directions across the whole operating current range. The extended near-field obtained

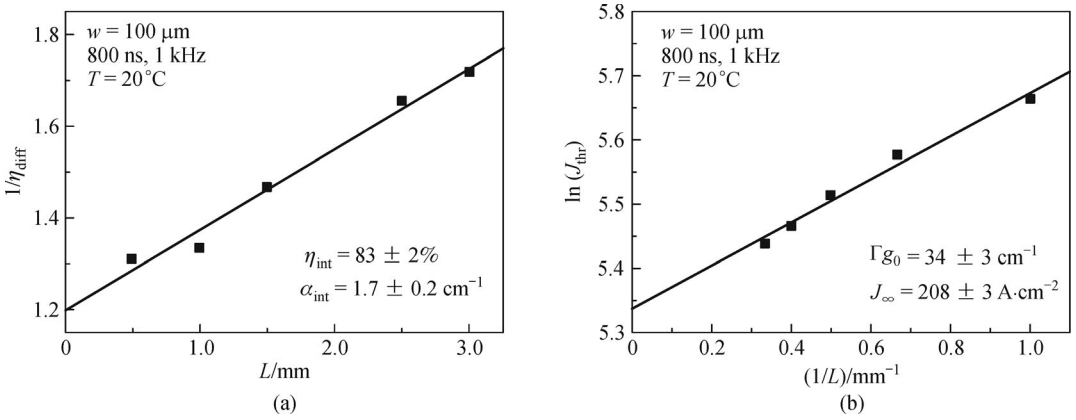

Fig. 18 (a) Reciprocal differential quantum efficiency as a function of cavity length; (b) threshold current density as a function of inverse cavity length

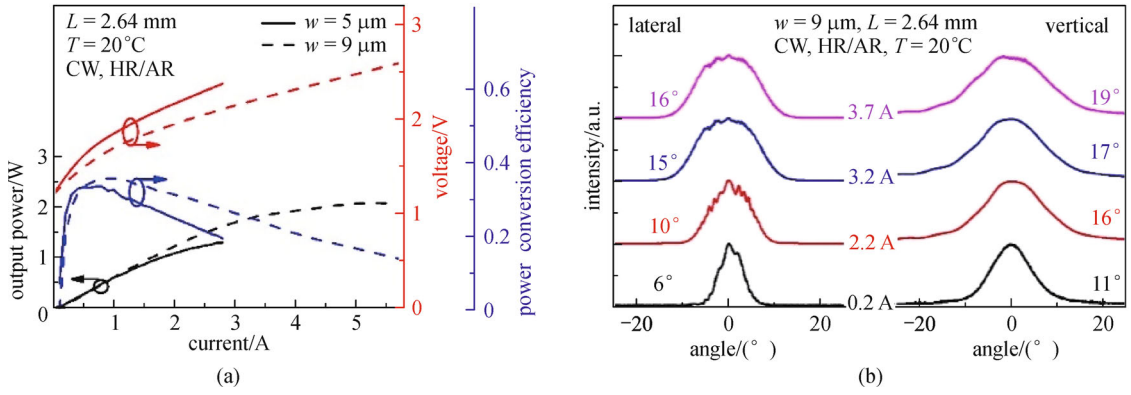

Fig. 19 (a) *L-I-V* characteristics and corresponding PCEs of a 5 μm and a 9 μm wide RW laser with 2.64 cavity length at $T = 20°C$ in CW mode. The laser facets are HR/AR coated; (b) far-field distributions of the 9 μm wide laser at different drive currents. FWHM beam divergence angles are indicated

by the thick vertical waveguide results in a narrow vertical beam divergence of only 12° at $I = 0.2$ A which increases to 16° at $I = 2.6$ A. The lateral FWHM beam divergence increases from 5° at $I = 0.2$ A also to 16° at $I = 2.6$ A resulting in a circular beam shape at $I = 2.6$ A, which is close to the allowed maximum current, as illustrated in Fig. 20(d).

5 Discussion and outlook

The 1060 nm PBC lasers presented here are of largest advantage for high power applications. Their high beam quality makes them also attractive for high brightness applications. Driving the lasers in the mode-locked regime extends their applicability to fields where high peak brightness is required. The robustness of the PBC structures against variations of the growth parameters makes the structures suitable for easy realization at different wavelength regimes. The performances of the already successful QW PBC structures can be enhanced further by using an active region with quantum dots (QDs). Deep 3D confinement potential of QDs would allow even higher current and thus higher power operation, since thermally induced carrier leakage would be reduced. The inherently suppressed charge carrier diffusion toward the facets in QD lasers increases the COMD level as compared to those of QW laser with otherwise identical vertical structure [41]. Lateral waveguiding technique could be combined with the PBC structures to improve beam quality further additionally increasing the brightness [42].

6 Conclusion

We presented a novel type of SL structure based on a PBC waveguide for high-power and brightness applications in the 1060 nm wavelength range. Record single transverse mode power of 1.9 W with narrow beam divergence of 9° in lateral and 14° in vertical directions is obtained for a

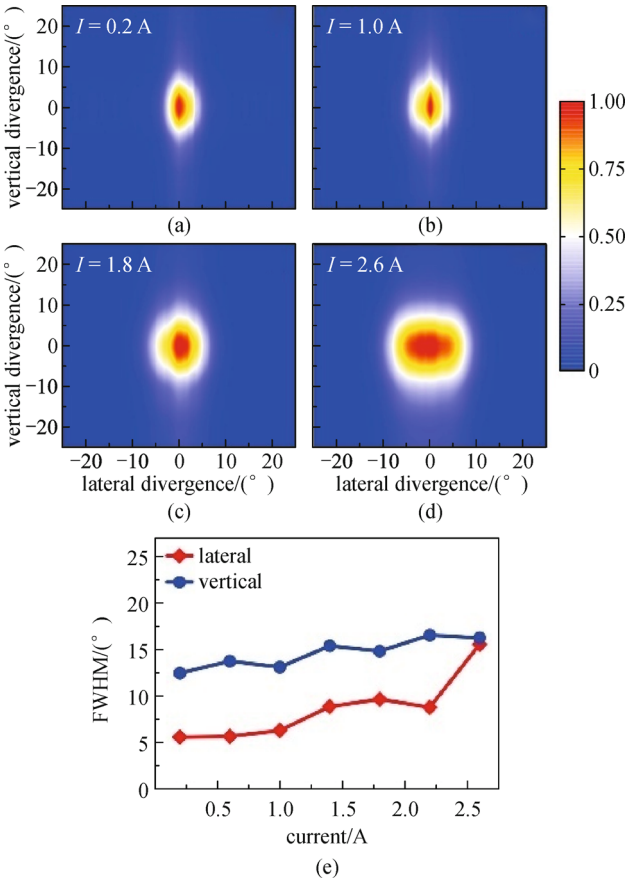

Fig. 20 Color-scale plot of CW-mode far-field distributions of the 5 μm wide RW laser at different drive currents in (a)–(d) at T = 20°C. FWHM beam divergence angle in lateral and vertical direction as function of operating current in (e)

vertically 15 μm thick PBC structure. Record peak brightness of 180 MW/cm^2/sr is achieved with 10 μm thick PBC lasers. A promising PBC waveguide having comparatively lower thickness and lower number of interfaces is presented. Despite presently still low internal efficiency, the lasers already provide similar output power and PCE as the thick waveguides. All these values are expected to increase further improving growth conditions. 1.3 W output power is delivered for a perfectly circular beam with narrow FWHM beam divergence of 16°.

Acknowledgements The authors acknowledge support of the German Research Council (DFG) within CRC 787. We are grateful to T. Kettler for laser processing, J. Pohl and M. Weyers for growth of the laser structures.

References

1. Inoue Y, Fujikawa S. Diode-pumped Nd:YAG laser producing 122-W CW power at 1.319 μm. IEEE Journal of Quantum Electronics, 2000, 36(6): 751–756
2. Schulz W, Poprawe R. Manufacturing with novel high-power diode lasers. IEEE Journal of Selected Topics in Quantum Electronics, 2000, 6(4): 696–705
3. Brauch U, Loosen P, Opower H. High-Power Diode Lasers: Fundamentals, Technology, Applications. In: Diehl R, ed. Berlin, Germany: Springer, 2000, 303–368
4. Hasler K H, Sumpf B, Adamiec P, Bugge F, Fricke J, Ressel P, Wenzel H, Erbert G, Tränkle G. 5-W DBR tapered lasers emitting at 1060 nm with a narrow spectral linewidth and a nearly diffraction-limited beam quality. IEEE Photonics Technology Letters, 2008, 20 (19): 1648–1650
5. Woods S. Understanding materials processing lasers. Laser-Technik-Journal, 2009, 6(5): 23–26
6. Lambert R W, Ayling T, Hendry A F, Carson J M, Barrow D A, McHendry S, Scott C J, McKee A, Meredith W. Facet-passivation processes for the improvement of Al-containing semiconductor laser diodes. Journal of Lightwave Technology, 2006, 24(2): 956–961
7. Murakami T, Ohtaki K, Matsubara H, Yamawaki T, Saito H, Isshiki K, Kokubo Y, Shima A, Kumabe H, Susaki W. A very narrow-beam AlGaAs laser with a thin tapered-thickness active layer (T^3 laser). IEEE Journal of Quantum Electronics, 1987, 23(6): 712–719
8. Yen S T, Lee C P. A novel cladding structure for semiconductor quantum-well lasers with small beam divergence and low threshold current. IEEE Journal of Quantum Electronics, 1996, 32(9): 1588–1595
9. Lin G, Yen S T, Lee C P, Liu D C. Extremely small vertical far-field angle of InGaAs-AlGaAs quantum-well lasers with specially designed cladding structure. IEEE Photonics Technology Letters, 1996, 8(12): 1588–1590
10. Yang G W, Xu J Y, Xu Z T, Zhang J M, Chen L H, Wang Q M. Theoretical investigation on quantum well lasers with extremely low vertical beam divergence and low threshold current. Journal of Applied Physics, 1998, 83(1): 8–14
11. Smowton P M, Lewis G M, Yin M, Summers H D, Berry G, Button C C. 650-nm lasers with narrow far-field divergence with integrated optical mode expansion layers. IEEE Journal of Selected Topics in Quantum Electronics, 1999, 5(3): 735–739
12. Bogatov A P, Gushchik T I, Drakin A E, Nekrasov A P, Popovichev V V. Optimisation of waveguide parameters of laser InGaAs/AlGaAs/GaAs heterostructures for obtaining the maximum beam width in the resonator and the maximum output power. Quantum Electronics, 2008, 38(10): 935–939
13. Crump P, Pietrzak A, Bugge F, Wenzel H, Erbert G, Tränkle G. 975 nm high power diode lasers with high efficiency and narrow vertical far field enabled by low index quantum barriers. Applied Physics Letters, 2010, 96(13): 131110–131110–3
14. Pietrzak A, Crump P, Wenzel H, Bugge F, Erbert G, Tränkle G. High power 1060 nm ridge waveguide lasers with low-index quantum barriers for narrow divergence angle. In: Proceedings of Conference on Lasers and Electro-Optics and Quantum Electronics and Laser Science. 2010, CWE2: 1–2
15. Pietrzak A, Crump P, Wenzel H, Erbert G. Combination of low-index quantum barrier and super large optical cavity designs for ultranarrow vertical far-fields from high-power broad-area lasers. IEEE Journal of Selected Topics in Quantum Electronics, 2011, 17 (6): 1715–1722
16. Shchukin V, Ledentsov N, Posilovic K, Kalosha V, Kettler T, Seidlitz D, Winterfeldt M, Bimberg D, Gordeev N Y, Karachinsky L

Y, Novikov I I, Shernyakov Y M, Chunareva A V, Maximov M V, Bugge F, Weyers M. Tilted wave lasers: a way to high brightness sources of light. IEEE Journal of Quantum Electronics, 2011, 47(7): 1014–1027

17. Kelemen M T, Weber J, Rinner F, Rogg J, Mikulla M, Weimann G. High-brightness 1040-nm tapered diode lasers. Proceedings of the Society for Photo-Instrumentation Engineers, 2003, 4947: 252–260
18. Kallenbach S, Kelemen M T, Aidam R, Lösch R, Kaufel G, Mikulla M, Weimann G. High-power high-brightness ridge-waveguide tapered diode lasers at 14xx nm. Proceedings of the Society for Photo-Instrumentation Engineers, 2005, 5738: 406–415
19. Kelemen M T, Weber J, Kallenbach S, Pfahler C, Mikulla M, Weimann G. Astigmatism and beam quality of high-brightness tapered diode lasers. Proceedings of the Society for Photo-Instrumentation Engineers, 2004, 5452: 233–243
20. Köhler B, Biesenbach J, Brand T, Haag M, Huke S, Noeske A, Seibold G, Behringer M, Luft J.High-brightness high-power kW-system with tapered diode laser bars. Proceedings of the Society for Photo-Instrumentation Engineers, 2005, 5711: 73–84
21. Ledentsov N N, Shchukin V A. Novel concepts for injection lasers. Optical Engineering, 2002, 41(12): 3193–3203
22. Bimberg D, Posilovic K, Kalosha V, Kettler T, Seidlitz D, Shchukin V A, Ledentsov N N, Gordeev N Yu, Karachinsky L Y, Novikov I I, Maximov M V, Shernyakov Y M, Chunareva A V, Bugge F, Weyers M. High-power high-brightness semiconductor lasers based on novel waveguide concepts. Proceedings of the Society for Photo-Instrumentation Engineers, 2010, 7616: 76161I
23. Kalosha V P, Posilovic K, Kettler T, Shchukin V A, Ledentsov N N, Bimberg D. Simulations of the optical properties of broad-area edge-emitting semiconductor lasers at 1060 nm based on the PBC laser concept. Semiconductor Science and Technology, 2011, 26(7): 075014
24. Maximov M V, Shernyakov Y M, Novikov I I, Kuznetsov S M, Karachinsky L Y, Gordeev N Y, Kalosha V P, Shchukin V A, Ledentsov N N. High-performance 640-nm-range GaInP-AlGaInP lasers based on the longitudinal photonic bandgap crystal with narrow vertical beam divergence. IEEE Journal of Quantum Electronics, 2005, 41(11): 1341–1348
25. Novikov I I, Karachinsky L Ya, Maximov M V, Shernyakov Yu M, Kuznetsov S M, Gordeev N Yu, Shchukin V A, Kopev P S, Ledentsov N N, Ben-Ami U, Kalosha V P, Sharon A, Kettler T, Posilovic K, Bimberg D, Mikhelashvili V, Eisenstein G. Single mode cw operation of 658 nm AlGaInP lasers based on longitudinal photonic band gap crystal. Applied Physics Letters, 2006, 88(23): 231108
26. Maximov M V, Shernyakov Yu M, Novikov I I, Kuznetsov S M, Karachinsky L Y, Gordeev N Y, Soshnikov I P, Musikhin Y G, Kryzhanovskaya N V, Sharon A, Ben-Ami U, Kalosha V P, Zakharov N D, Werner P, Kettler T, Posilovic K, Shchukin V A, Ledentsov N N, Bimberg D. Longitudinal photonic bandgap crystal laser diodes with ultra-narrow vertical beam divergence. In: Proceedings of Physics & Simulation of Optoelectronic Devices XIV. 2006, 6115: 611513
27. Maximov M V, Shernyakov Y M, Novikov I I, Karachinsky L Y, Gordeev N Y, Ben-Ami U, Bortman-Arbiv D, Sharon A, Shchukin V A, Ledentsov N N, Kettler T, Posilovic K, Bimberg D. High-power low-beam divergence edge-emitting semiconductor lasers with 1- and 2-D photonic bandgap crystal waveguide. IEEE Journal of Selected Topics in Quantum Electronics, 2008, 14(4): 1113–1122
28. Posilovic K, Kettler T, Shchukin V A, Ledentsov N N, Pohl U W, Bimberg D, Fricke J, Ginolas A, Erbert G, Tränkle G, Jönsson J, Weyers M. Ultrahigh-brightness 850 nm GaAs/AlGaAs photonic crystal laser diodes. Applied Physics Letters, 2008, 93(22): 221102
29. Novikov I I, Gordeev N Yu, Shernyakov Y M, Kiselev Yu Yu, Maximov M V, Kopev P S, Sharon A, Duboc R, Arbiv D B, Ben-Ami U, Shchukin V A, Ledentsov N N. High-power single mode ($>>1$ W) continuous wave operation of longitudinal photonic band crystal lasers with a narrow vertical beam divergence. Applied Physics Letters, 2008, 92(10): 103515
30. Kettler T, Posilovic K, Karachinsky L Y, Ressel P, Ginolas A, Fricke J, Pohl U W, Shchukin V A, Ledentsov N N, Bimberg D, Jönsson J, Weyers M, Erbert G, Tränkle G. High-brightness and ultranarrow-beam 850-nm GaAs/AlGaAs photonic band crystal lasers and single-mode arrays. IEEE Journal of Selected Topics in Quantum Electronics, 2009, 15(3): 901–908
31. Posilovic K, Kalosha V P, Winterfeldt M, Schulze J H, Quandt D, Germann T D, Strittmatter A, Bimberg D, Pohl J, Weyers M. High-power low-divergence 1060 nm photonic crystal laser diodes based on quantum dots. Electronics Letters, 2012, 48(22): 1419–1420
32. Miah M J, Kettler T, Posilovic K, Kalosha V P, Skoczowsky D, Rosales R, Bimberg D, Pohl J, Weyers M. 1.9 W continuous-wave single transverse mode emission from 1060 nm edge-emitting lasers with vertically extended lasing area. Applied Physics Letters, 2014, 105(15): 151105
33. Rosales R, Kalosha V P, Posilovic K, Miah M J, Bimberg D, Pohl J, Weyers M. High brightness photonic band crystal semiconductor lasers in the passive mode locking regime. Applied Physics Letters, 2014, 105(16): 161101
34. Miah M J, Kettler T, Kalosha V P, Posilovic K, Bimberg D, Pohl J, Weyers M. High temperature operation of 1060-nm high-brightness photonic band crystal lasers with very low astigmatism. IEEE Journal of Selected Topics in Quantum Electronics, 2015, 21(6): 4900206
35. Kalosha V P, Bimberg D. Device comprising a high brightness broad-area edge-emitting semiconductor laser and method of making the same. 2014, U.S. patent application, US20150288147
36. Numai T. Fundamentals of Semiconductor Lasers. In: Rhodes W T, ed. Berlin, Germany: Springer, 2004, 97–100
37. Agrawal G P, Dutta N K. Semiconductor Lasers. 3rd ed. Boston, MA, USA: Kluwer, 2001, 132–139
38. Wenzel H, Bugge F, Dallmer M, Dittmar F, Fricke J, Hasler K H, Erbert G. Fundamental-lateral mode stabilized high-power ridge-waveguide lasers with a low beam divergence. IEEE Photonics Technology Letters, 2008, 20(3): 214–216
39. Tai K, Yang L, Wang Y H, Wynn J D, Cho A Y. Drastic reduction of series resistance in doped semiconductor distributed Bragg reflectors for surface-emitting lasers. Applied Physics Letters, 1990, 56(25): 2496–2498
40. Wenzel H, Dallmer M, Erbert G. Thermal lensing in high-power ridge-waveguide lasers. Optical and Quantum Electronics, 2008, 40 (5): 379–384
41. Sellin R L, Ribbat C, Bimberg D, Rinner F, Konstanzer H, Kelemen

M T, Mikulla M. High-reliability MOCVD-grown quantum dot laser. Electronics Letters, 2002, 38(16): 883–884

42. Kalosha V P, Posilovic K, Bimberg D. Lateral-longitudinal modes of high-power inhomogeneous waveguide Lasers. IEEE Journal of Quantum Electronics, 2012, 48(2): 123–128

Md. Jarez Miah received the B.Sc. degree in electrical and electronic engineering from Bangladesh University of Engineering and Technology, Dhaka, Bangladesh, in 2009 and the M.Sc. degree in communications technology from Ulm University, Ulm, Germany, in 2012. He is currently working toward the Ph.D. degree at the Institute of Solid State Physics, Technical University of Berlin, Berlin, Germany. His research interests include design, fabrication and characterization of high-power and high-brightness semiconductor lasers.

He received the "Best Student Award 2011" from Ulm University in 2011 and was the recipient of "Einstein Scholarship 2010" from the Ulmer Universitätsgesellschaft, Germany.

Vladimir P. Kalosha received the M.S. degree in theoretical physics, the Ph.D. degree in waveguide theory and fiber optics, and the Dr.Sc. degree in solid-state laser physics from Belarus State University, Minsk, in 1977, 1984 and 1994, respectively. He was with the Institute of Applied Physics Problems, Belarus State University, from 1977 to 1991, eventually rising to the position of Senior Research Officer and he held the position of Head of the Laser Optics Laboratory in the International Laser Center, Belarus State University, from 1991 to 1995. He was with the Max Born Institute for Nonlinear Optics and Short-Pulse Spectroscopy, Berlin, Germany, as a Visiting Scientist and Researcher until 2004. In 2001, he was the Director of Modeling of VPISystems Inc., Berlin. From 2004 to 2008, he was a Senior Research Fellow in the Fiber Optics Group, Department of Physics, University of Ottawa, ON, Canada. He is with the Institute for Solid-State Physics, Technical University of Berlin, Berlin, Germany since 2009. He has authored or coauthored over 150 papers, book chapters, patents and conference presentations. His current research interests include a wide array of topics at the crossroads of nonlinear optics, ultrafast phenomena, solid-state, fiber, semiconductor lasers, innovative optical networks, and components. Dr. Kalosha was awarded the Alexander von Humboldt Fellowship from 1996 to 1997.

Ricardo Rosales received the Ph.D. degree in 2012 from the University Pierre et Marie Curie, France, after finishing his research work on InAs/InP quantum dash mode locked lasers for optical communications at the Laboratory for Photonics and Nanostructures (LPN-CNRS). He is now a postdoctoral researcher at the Technical University of Berlin, Germany, where he is involved in the development of novel high brightness semiconductor lasers for high power optical pulse generation.

Dieter H. Bimberg received the Diploma in physics and Ph.D. degree from Goethe University, Frankfurt, in 1968 and 1971, respectively. From 1972 to 1979, he held a Principal Scientist position at the Max Planck-Institute for Solid State Research in Grenoble/France and Stuttgart. In 1979, he was appointed as Professor of Electrical Engineering, Technical University of Aachen. In 1981, he was appointed to the Chair of Applied Solid State Physics at Technical University of Berlin. He was elected in 1990 Excecutive Director of the Solid State Physics Institute at TU Berlin, a position he hold until 2011. In 2004, he founded the Center of Nanophotonics at TU Berlin. From 2006 to 2011, he was the chairman of the board of the German Federal Government Centers of Excellence in Nanotechnologies.

His honors include the Russian State Prize in Science and Technology 2001, his election to the German Academy of Sciences Leopoldina in 2004, to the Russian Academy of Sciences in 2011, and to the US National Academy of Engineering in 2014, as Fellow of the American Physical Society and IEEE in 2004 and 2010, respectively, the Max-Born-Award and Medal 2006, awarded jointly by IoP and DPG, the William Streifer Award of the Photonics Society of IEEE in 2010, the UNESCO Nanoscience Medal 2012, and the Heinrich-Welker-Award and medal in 2015. The University of Lancaster bestowed in 2015 the D.Sc.h.c. to him.

He has authored more than 1200 papers, 25 patents, and 6 books resulting in more than 48000 citations worldwide and a Hirsch factor of 98.

His research interests include the growth and physics of nanostructures and nanophotonic devices, ultrahigh speed and energy efficient photonic devices for future datacom systems, single/entangled photon emitters for quantum cryptography and ultimate nanomemories based on quantum dots.